Sensors and Materials, Vol. 33, No. 6 (2021) 2215–2226
MYU Tokyo

S & M 2610

Scintillation Properties of Non-doped and Pr-doped $BaO–B_2O_3–SiO_2$ Glasses and Glass-ceramics

Noriaki Kawaguchi,[1*] Hirokazu Masai,[2] Masaki Akatsuka,[1]
Daisuke Nakauchi,[1] Takumi Kato,[1] and Takayuki Yanagida[1]

[1]Nara Institute of Science and Technology, 8916-5 Takayama-cho, Ikoma, Nara 630-0192, Japan
[2]National Institute of Advanced Industrial Science and Technology,
1-8-31 Midorigaoka, Ikeda, Osaka 563-8577, Japan

(Received February 3, 2021; accepted June 1, 2021)

Keywords: scintillator, glass-ceramics, luminescence

We have studied the scintillation properties of non-doped and Pr-doped $BaO–B_2O_3–SiO_2$ glasses and glass-ceramics. The glass transition temperature (T_g), the temperature of crystallization onset (T_x), and the crystallization peak (T_p) were determined by differential thermal analysis. The glass-ceramics were obtained by heating at three different temperatures (T_g + 50 °C, T_x, and T_p). We confirmed that the X-ray diffraction peaks can be ascribed to the $BaSiO_3$ crystalline phase in the glass-ceramic samples. In the X-ray-induced scintillation spectra, we observed the intrinsic luminescence of the host glass and luminescence due to the 4f–4f transition of Pr^{3+} ions. In addition, the 1% Pr-doped $BaO–B_2O_3–SiO_2$ glass-ceramic with heating at T_g + 50 °C clearly showed luminescence in the wavelength range from 250 to 350 nm under X-ray excitation. Its photoluminescence (PL) decay time was estimated to be 26.28 ns and its luminescence is considered to be due to the 5f–4f transition of Pr^{3+} ions.

1. Introduction

Radiation detectors and dosimeters are widely utilized for medical, industrial, and scientific applications. Whereas radiation detectors can immediately detect ionizing radiation, dosimeters can record the information of radiation doses over a certain period of time. Some radiation detectors and dosimeters use phosphor materials such as scintillators and dosimetric materials.

Scintillators[1–6] are materials that emit light in response to incident ionizing radiation and are widely used for non-destructive inspection,[7,8] medical imaging,[9] and well logging[10,11] applications using ionizing radiation. The properties required for scintillators are a high light yield, a fast decay time, and a high effective atomic number. Dosimetric materials[12] can be classified into three types: thermoluminescence (TL),[13] optically stimulated luminescence (OSL),[14,15] and radio-photoluminescence (RPL)[16–18] materials. The main properties required for dosimetric materials are a wide measurable range and human tissue equivalency.

There have been many studies on the properties of scintillators and dosimetric materials in the last several decades,[2–6,12] and research on both types of phosphor materials is still an

*Corresponding author: e-mail: n-kawaguchi@ms.naist.jp
https://doi.org/10.18494/SAM.2021.3410

ISSN 0914-4935

attractive topic. As recent studies on scintillators and dosimetric materials, single crystals,[19–31] sintered ceramics,[32–37] glasses,[38–43] eutectics,[44,45] plastics,[46] and organic-inorganic hybrid materials[47] have been reported. Among them, glass materials have the advantages of high transparency, formability, and chemical stability. The disadvantage of glass materials is their lower luminescence efficiency than those of single-crystalline materials. A possible method to improve the luminescence properties of glass materials is the crystallization of glasses.

Crystallized glasses can have high translucency and contain crystallites in their glass matrix, which are called glass-ceramics. They have optical, medical, electronic, and military applications and are also used in kitchenware. Although no glass-ceramics are widely used as scintillators and dosimetric materials, a few interesting studies have been performed. For example, the germanate glass-ceramic containing $Bi_4Ge_3O_{12}$ crystallites,[48] the fluorophosphate glass-ceramic containing CeF_3 crystallites,[49] oxyfluoride glass-ceramics containing CaF_2:Eu crystallites,[50,51] and oxyfluoride glass-ceramics containing $CeBr_3$ crystallites[52] have been studied. Our group is also focusing on glass-ceramics as scintillators and dosimetric materials, and we have already shown an increase in the scintillation and TL intensities of 20SrO-20BaO-40Nb_2O_5-20P_2O_5 glass upon its crystallization.[53] However, there have been relatively few studies on glass-ceramic scintillators and dosimetric materials compared with those on single-crystalline materials, and further studies on glass-ceramic materials are desirable.

In this study, we focus on glass-ceramics containing Pr-doped $BaSiO_3$ crystallites for scintillator applications. Since Ba is a heavy element, it is expected that Ba-rich glasses can exhibit a high effective atomic number. Furthermore, luminescence due to the 5d–4f transitions of Pr^{3+} ions can show a fast decay time. Because it is difficult to obtain transparent 50BaO-50SiO_2 glass with the stochiometric chemical composition of $BaSiO_3$, we added a small amount of B_2O_3. Therefore, the compositions of non-doped and Pr-doped 47.5BaO-5B_2O_3-47.5SiO_2 glasses and glass-ceramics were investigated.

2. Materials and Methods

Non-doped and Pr-doped 47.5BaO-5B_2O_3-47.5SiO_2 glasses (hereinafter referred to as BaO–B_2O_3–SiO_2 glasses) were prepared using a conventional melt-quenching method. The Pr ions were doped with 0.1, 0.5, and 1 mol% of the total amount of cations. High-purity Pr_6O_{11} (99.9%), $BaCO_3$ (99.95%), B_2O_3 (99.9%), and SiO_2 (99.999%) powders were used as starting materials. The powders were mixed and loaded into a platinum crucible, then melted at 1600 °C for 30 min using an electric furnace under ambient atmosphere. The melt was quenched on a stainless steel plate maintained at 200 °C.

Small pieces were taken from the obtained glasses and used for differential thermal analysis (DTA) measurements. The DTA curves of the non-doped and Pr-doped BaO–B_2O_3–SiO_2 glasses were measured at a heating rate of 10 °C/min using a DTA measurement system (Thermo plus EVO2/TG-DTA8120; Rigaku, Akishima, Japan). The glass transition temperature (T_g), the temperature of crystallization onset (T_x), and the crystallization peak (T_p) of each glass were determined from the obtained DTA curves using the data analysis software for Thermo plus EVO2/TG-DTA8120.

The glass pieces that were not used for DTA measurements were annealed at T_g under ambient atmosphere for stress relaxation. The annealed glasses were cut into pieces of approximately 10 × 10 × 1 mm^3 and mechanically polished. The obtained glass pieces were individually heated at three different temperatures (T_g + 50 °C, T_x, and T_p) in ambient atmosphere with a holding time of 3 h to induce the nucleation and growth of crystallites using the electric furnace.

The crystalline phases of the samples were identified by X-ray diffraction (XRD). The XRD patterns of the samples were measured using an X-ray diffractometer equipped with a Cu-Kα X-ray source (MiniFlex600; Rigaku). Crystal phases were identified using the Powder Diffraction File (PDF) from the International Centre for Diffraction Data (ICDD). To investigate the optical properties, diffuse transmittance spectra of the samples were measured using a UV-VIS-NIR spectrophotometer (SolidSpec-3700; SHIMADZU, Kyoto, Japan) across the spectral range from 200 to 800 nm. Backscattered electron images were obtained using a desktop scanning electron microscope (JCM-6000Plus; JEOL, Akishima, Japan) to observe the microstructures of the samples.

To investigate the scintillation properties, X-ray-induced scintillation spectra of the samples were measured using our customized setup comprising an X-ray generator, an optical fiber, and a spectrometer, as described in detail elsewhere.[54] X-rays were irradiated to the samples from the X-ray generator (XRB80P&N200X4550; Spellman High Voltage Electronics, New York, United States), and then emissions from the samples were guided to the monochromator (Shamrock 163; Andor Technology, Belfast, UK) with a CCD-based spectrometer (DU920-BU2NC; Andor Technology). The X-ray generator was operated with a tube voltage of 80 kV and a tube current of 1.2 mA. In addition, we measured the photoluminescence (PL) decay curve of the 1% Pr-doped sample heated at T_g + 50 °C using a fluorescence lifetime spectrometer (Quantaurus-Tau C11367; Hamamatsu Photonics, Hamamatsu, Japan) to consider the origin of scintillation in the UV range.

3. Results and Discussion

Figure 1 shows the DTA curves of the non-doped and Pr-doped $BaO–B_2O_3–SiO_2$ glasses. Exothermic peaks due to glass crystallization were clearly observed. The DTA curves are shown with two different scales because the exothermic peaks were high. The crystallization peak was strong because these compositions were easily crystallized. This is consistent with the fact that the transparent $50BaO\text{-}50SiO_2$ glass was difficult to obtain. Although we added a small amount of B_2O_3 to obtain the transparent glasses, the samples still showed strong peaks due to glass crystallization.

The T_g, T_x, and T_p values were determined from the DTA curves. T_g and T_x are shown in Fig. 1(a) and T_p is shown in Fig. 1(b). The T_g value was determined as the temperature of the intersection between the tangent line to the initial baseline and that to the first slope. Similarly, the T_x value was determined as the temperature of the intersection between the tangent line to the gentle slope before the exothermic peak due to glass crystallization and that to the rising slope of this exothermic peak. The T_p value was determined as the temperature of this exothermic peak. Table 1 shows the thermal properties of the non-doped and Pr-doped $BaO–B_2O_3–SiO_2$

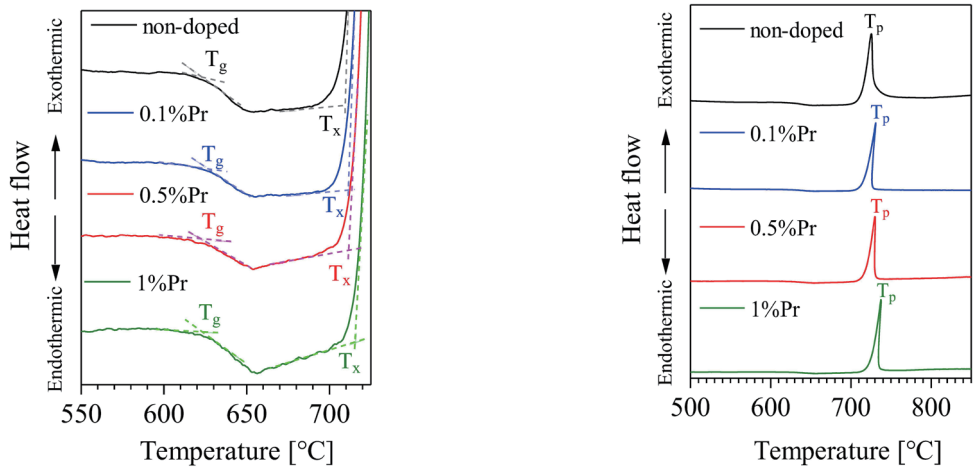

Fig. 1. (Color online) DTA curves of non-doped and Pr-doped $BaO–B_2O_3–SiO_2$ glasses showing (a) the glass transition temperature (T_g) and the temperature of crystallization onset (T_x) and (b) the crystallization peak (T_p).

Table 1
Thermal properties of the non-doped and Pr-doped $BaO–B_2O_3–SiO_2$ glasses.

	T_g (°C)	T_x (°C)	T_p (°C)	ΔT (= $T_x - T_g$) (°C)
non-doped	623	710	726	87
0.1% Pr	624	712	731	88
0.5% Pr	622	712	730	90
1% Pr	622	715	738	93

glasses. T_g, T_x, and T_p of the non-doped $BaO–B_2O_3–SiO_2$ glass were 623, 710, and 726 °C, respectively. The glass with the highest Pr-doping concentration (the 1% Pr-doped $BaO–B_2O_3–SiO_2$ glass) showed T_g, T_x, and T_p of 622, 715, and 738 °C, respectively. It was revealed that T_g of the samples did not depend on the Pr-doping concentration. In contrast, T_x and T_p increased with increasing Pr-doping concentration. Since ΔT (= $T_x - T_g$) increased with increasing Pr-doping concentration, Pr doping seemed to slightly contribute to the increased thermal stability of the $BaO–B_2O_3–SiO_2$ glass upon crystallization.

Figure 2 shows the appearance of the non-doped and Pr-doped $BaO–B_2O_3–SiO_2$ glasses and glass-ceramics. All the samples were transparent or translucent. Since all the samples were successfully cut and polished to a size of approximately 10 × 10 × 1 mm^3 with no visible large cracks, the annealing temperatures were considered to be suitable. The non-heated samples showed high transparency and a green color due to Pr doping. In addition, the heated samples were opaque, possibly due to scattering centers. The samples heated at higher temperatures became more opaque. The samples obtained with heating at T_x, and T_p were more opaque than those heated at T_g + 50 °C; however, no difference between the opacities of the samples heated to T_x and T_p was visually observed.

The crystalline phases of the samples were determined by XRD. Figure 3 shows XRD patterns of the non-doped and 1% Pr-doped $BaO–B_2O_3–SiO_2$ glasses and glass-ceramics.

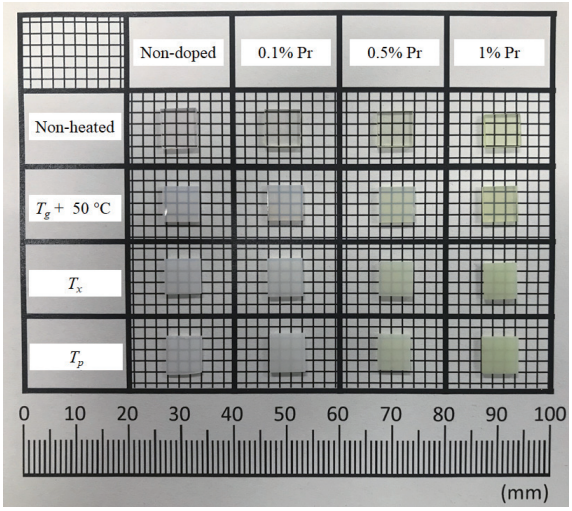

Fig. 2. (Color online) Non-doped and Pr-doped $BaO–B_2O_3–SiO_2$ glasses and glass-ceramics.

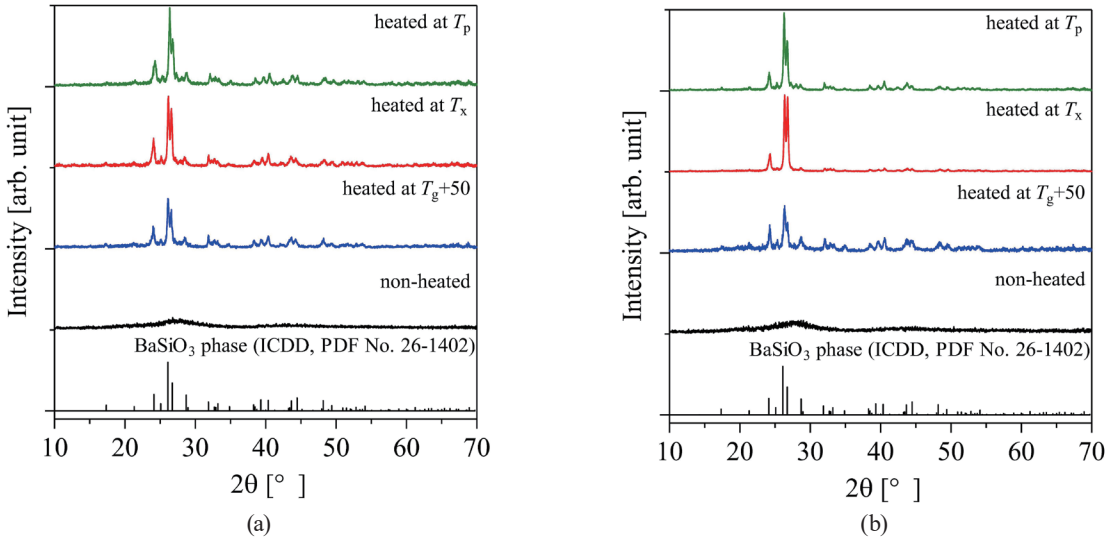

Fig. 3. (Color online) XRD patterns of (a) non-doped and (b) 1% Pr-doped $BaO–B_2O_3–SiO_2$ glasses and glass-ceramics.

Whereas the XRD patterns of the non-heated glass samples only showed halo patterns, the heated glass-ceramic samples showed XRD peaks ascribed to the $BaSiO_3$ phase (ICDD, PDF No. 26-1402) as shown in the figure. No significant differences in the crystalline phases were observed between the non-doped and 1% Pr-doped samples, and no Pr-related crystalline phases were observed. It is possible that the Pr element was contained in both the glass matrix and the $BaSiO_3$ crystallites. None of the XRD patterns of the heated samples showed clear halo peaks. However, it is possible that the XRD patterns of the weak halo peaks overlapped because the intensities of the halo patterns produced by the $BaO–B_2O_3–SiO_2$ glasses were significantly lower than those produced by the $BaSiO_3$ crystalline phases.

Figure 4 shows the diffuse transmittance spectra of the samples. The Pr-doped samples showed absorption bands of Pr^{3+} ions at around 450 and 600 nm. Furthermore, the samples heated at higher temperatures showed lower transmittance due to the scattering by $BaSiO_3$ crystallites. Here, Rayleigh scattering, which is scattering by particles with a small size compared with the wavelength of visible light, should be considered. Assuming independent spherical particles, the scattering cross section σ_s given by Rayleigh can be written as

$$\sigma_s \propto \frac{\alpha^6}{\lambda^4}, \tag{1}$$

where λ is the wavelength and α is the radius of the scattering material.[55] In the case of glass-ceramics, the scattering material is the crystallites contained in the glass. If α is not sufficiently smaller than λ, then glass-ceramics are not transparent in the short-wavelength range. Here, we confirmed a significant decrease in the diffuse transmittance of the samples in the short-wavelength range, which was due to Rayleigh scattering by the crystallites.

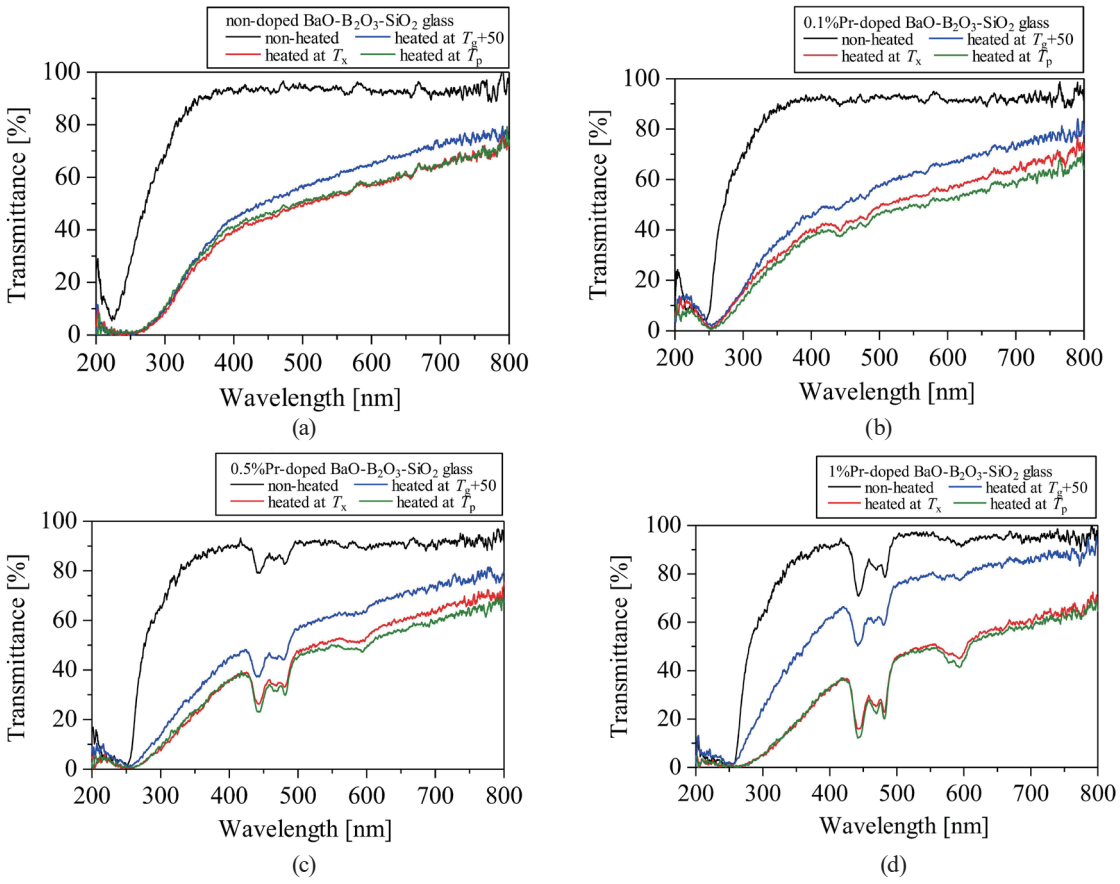

Fig. 4. (Color online) Diffuse transmittance spectra of (a) non-doped, (b) 0.1% Pr-doped, (c) 0.5% Pr-doped, and (d) 1% Pr-doped $BaO–B_2O_3–SiO_2$ glasses and glass-ceramics.

Furthermore, the samples obtained with heating at T_g + 50 °C tended to show higher transmittance than the samples obtained with heating at T_x and T_p. In particular, this tendency was clearly confirmed in the 1% Pr-doped $BaO–B_2O_3–SiO_2$ glass-ceramics. Figure 5 shows backscattered electron images of the 1% Pr-doped $BaO–B_2O_3–SiO_2$ glasses obtained with heating at T_g + 50, T_x, and T_p. It was observed that the 1% Pr-doped $BaO–B_2O_3–SiO_2$ glass-ceramic obtained with heating at T_g + 50 °C had fewer grains than the other samples. This is the reason why the 1% Pr-doped $BaO–B_2O_3–SiO_2$ glass-ceramic showed relatively high transmittance.

Figure 6 shows X-ray-induced scintillation spectra of the samples. All the non-doped samples showed a similar broad emission band from 300 to 600 nm, which is considered to have originated from the intrinsic luminescence of the host glass. In general, intrinsic luminescence can be observed in non-doped oxide glasses. As the origin of such intrinsic luminescence, for example, the luminescence related to radiative annihilation of the self-trapped excitons and the luminescence due to the recombination of electrons with O^- hole centers have been considered.(56) The Pr-doped samples showed emission peaks at around 450, 500, and 600 nm, overlapping with the broad emission from 300 to 600 nm. These peaks are considered to originate from the 4f–4f transition of Pr^{3+} ions. The scintillation intensities of the samples obtained with heating at T_x and T_p tended to be lower than those of the non-heated samples. This is consistent with the decrease in the transmittances of the samples obtained with heating at T_x and T_p. Although the scintillation intensities of glasses can be sometimes enhanced by crystallization,(53) the effect of a decrease in transmittance seems to be dominant in this study. Furthermore, some of the heated Pr-doped samples showed a broad emission band from 250 to 350 nm, which was not observed in the non-doped and non-heated samples. This was particularly apparent in the 0.5 and 1% Pr-doped $BaO–B_2O_3–SiO_2$ glass-ceramics obtained with heating at T_g + 50 °C. These samples also showed relatively high transmittance in the short wavelength range as shown in Fig. 4. The clear observation of this emission band is considered to be due to their higher transparency in the short wavelength range compared with the other heated samples. Moreover, we propose that its origin was the emission from Pr-doped $BaSiO_3$ because it was clearly observed only in the heated Pr-doped samples.

Figure 7 shows the PL emission and excitation spectra of the 1% Pr-doped $BaO–B_2O_3–SiO_2$ glass-ceramic obtained with heating at T_g + 50 °C, the 1% Pr-doped $BaO–B_2O_3–SiO_2$ glass, and

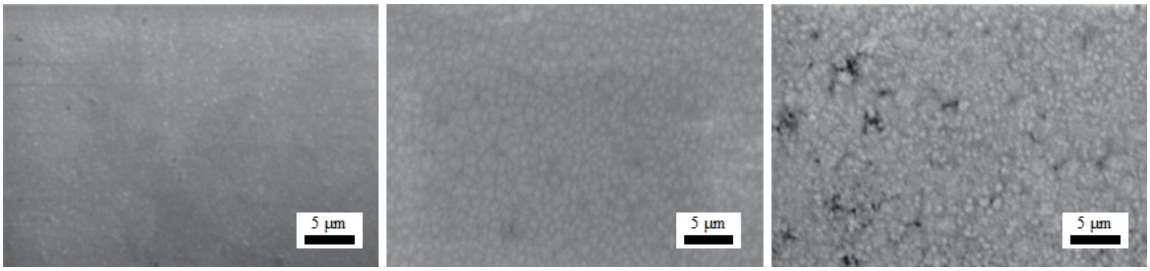

(a) (b) (c)

Fig. 5. Backscattered electron images of the 1% Pr-doped $BaO–B_2O_3–SiO_2$ glasses obtained with heating at (a) T_g + 50, (b) T_x, and (c) T_p.

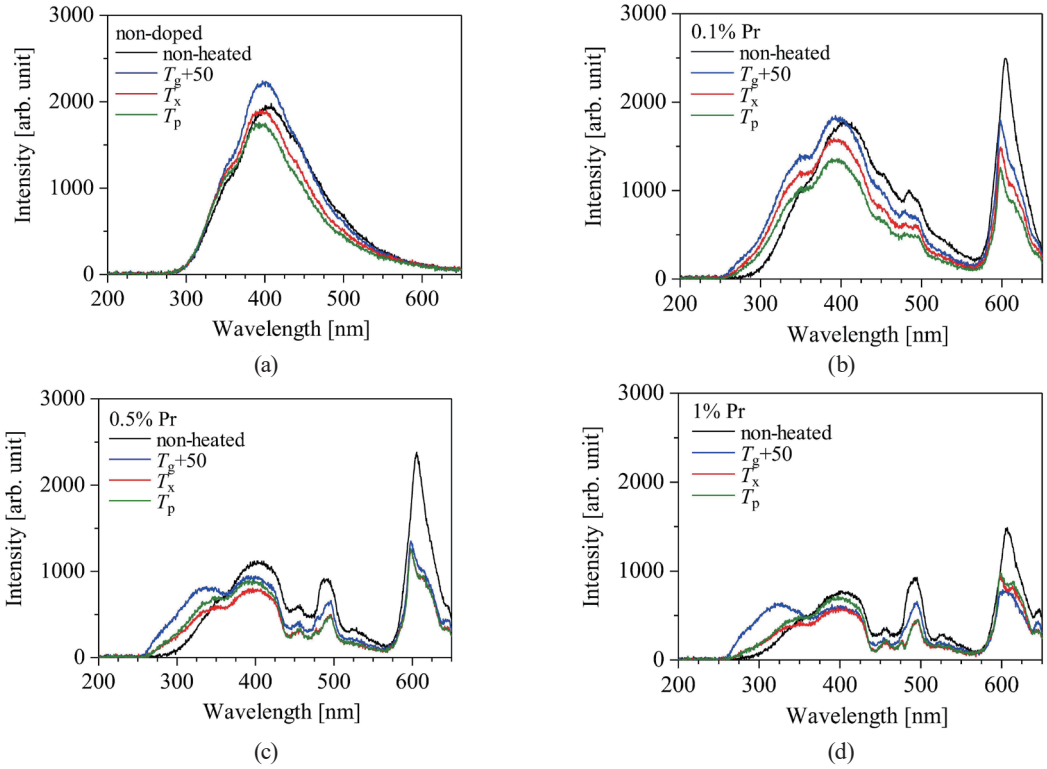

Fig. 6. (Color online) X-ray-induced scintillation spectra of (a) non-doped, (b) 0.1% Pr-doped, (c) 0.5% Pr-doped, and (d) 1% Pr-doped $BaO–B_2O_3–SiO_2$ glasses and glass-ceramics.

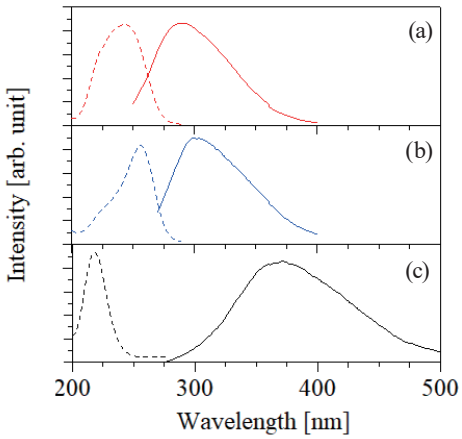

Fig. 7. (Color online) PL emission (solid line) and excitation (dashed line) spectra of (a) the 1% Pr-doped $BaO–B_2O_3–SiO_2$ glass-ceramic obtained with heating at T_g + 50 °C, (b) the 1% Pr-doped $BaO–B_2O_3–SiO_2$ glass, and (c) the non-doped $BaO–B_2O_3–SiO_2$ glass. The emission spectra were obtained with excitation wavelengths of (a) 240, (b) 250, and (c) 214 nm. The excitation spectra were obtained with emission wavelengths of (a) 310, (b) 310, and (c) 360 nm.

the non-doped $BaO–B_2O_3–SiO_2$ glass. The non-doped $BaO–B_2O_3–SiO_2$ glass clearly showed a shorter excitation wavelength and a longer emission wavelength than those of the other samples. Their origin was considered to be the excitation and emission bands of the intrinsic luminescence in the $BaO–B_2O_3–SiO_2$ glass.

The emission peaks of the 1% Pr-doped $BaO–B_2O_3–SiO_2$ glass and 1% Pr-doped $BaO–B_2O_3–SiO_2$ glass-ceramic obtained with heating at T_g + 50 °C were around 300 and 290 nm, respectively. Since their excitation spectra seem to have two components, we fitted the excitation spectra to the sum of two Gaussian functions. Whereas the excitation spectrum of the non-heated 1% Pr-doped $BaO–B_2O_3–SiO_2$ glass had components with peaks at 240.0 and 257.6 nm, that of the 1% Pr-doped $BaO–B_2O_3–SiO_2$ glass-ceramic obtained with heating at T_g + 50 °C had components with peaks at 226.3 and 248.7 nm. Therefore, the glass-ceramic sample showed shorter emission and excitation wavelengths. These components appear to be due to the luminescence associated with the 5d–4f transition of Pr^{3+} ions because their emission wavelengths were shorter than the other emission peaks and the Stokes shifts were small. The difference in the emission and excitation wavelengths between the samples can also be explained because the emission and excitation wavelengths associated with the 5d–4f transition of Pr^{3+} ions generally depend on the host material, in contrast to those associated with the 4f–4f transition of Pr^{3+} ions. We believe that the shorter emission and excitation wavelengths originated from the 5d–4f transition of Pr^{3+} ions in the $BaSiO_3$ crystalline phase. To the best of our knowledge, the emission spectrum of Pr-doped $BaSiO_3$ in the wavelength range from 250 to 350 nm has not been reported; however, there has been a study on the broad emission band around 300 nm of Pr-doped $CaSiO_3$.[57] This similar oxide compound shows luminescence due to the 5d–4f transition of Pr^{3+} ions. Therefore, it is a possible explanation for the origin of the luminescence.

To discuss the origin of the luminescence on the basis of the decay time, the PL decay curve was measured. Figure 8 shows the PL decay curve of the 1% Pr-doped $BaO–B_2O_3–SiO_2$ glass-ceramic obtained with heating at T_g + 50 °C. In this experiment, the excitation and observation wavelengths were 280 and 310 nm, respectively (the shortest excitation wavelength of our PL spectrometer was 280 nm). The obtained decay curve was well fit by a triple exponential function. The estimated decay times were 1.610, 6.772, and 26.28 ns. The faster decay components of 1.610 and 6.772 ns were considered to be due to the instrumental response function (IRF). The decay time of 26.28 ns is a typical value for the 5d–4f transition of Pr^{3+} ions.[58] Because no other slower components were observed, this result seems to be consistent with the discussion of the PL emission and excitation spectra.

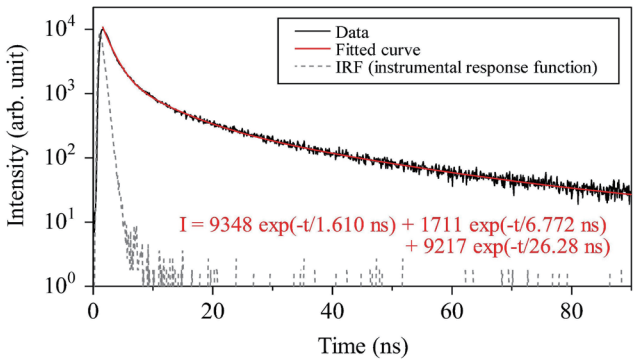

Fig. 8. (Color online) PL decay curve of the 1% Pr-doped $BaO–B_2O_3–SiO_2$ glass-ceramic obtained with heating at T_g + 50 °C under an excitation wavelength of 280 nm and an observation wavelength of 310 nm.

Although samples with fast decay times can be useful for scintillator applications, the scintillation intensities of the samples in the wavelength range from 250 to 350 nm were low. Further studies are needed to increase the scintillation intensity of the Pr-doped glass-ceramics while maintaining the fast decay time.

4. Conclusions

The scintillation properties of non-doped and Pr-doped $BaO–B_2O_3–SiO_2$ glasses and glass-ceramics were studied. In the DTA curves of the non-doped and Pr-doped $BaO–B_2O_3–SiO_2$ glasses, we observed exothermic peaks due to glass crystallization and estimated the T_g, T_x, and T_p values. ΔT (= T_x – T_g) of the 1% Pr-doped $BaO–B_2O_3–SiO_2$ glass was higher than that of the other samples. This result indicates that Pr doping improves the thermal stability of $BaO–B_2O_3–SiO_2$ glasses against crystallization. In the diffuse transmittance spectra of the samples, we observed a decrease in transmittance due to crystallization. $BaSiO_3$ crystalline phases were confirmed in the heated non-doped and Pr-doped $BaO–B_2O_3–SiO_2$ glasses by XRD. Among the glass-ceramics samples, those obtained with heating at T_g + 50 °C (the lowest heating temperature in this study) showed the highest transmittance. This is because the crystallization at T_g + 50 °C proceeded less than that at T_x and T_p. This was confirmed by backscattered electron images.

In the X-ray-induced scintillation spectra, the heated and non-heated $BaO–B_2O_3–SiO_2$ glasses showed intrinsic luminescence in the wavelength range from 300 to 600 nm. The Pr-doped $BaO–B_2O_3–SiO_2$ glasses and glass-ceramics showed luminescence due to the 4f–4f transition of Pr^{3+} ions. The luminescence due to the 5d–4f transition of Pr^{3+} ions was also observed, particularly in the 0.5 and 1% Pr-doped $BaO–B_2O_3–SiO_2$ glass-ceramics obtained with heating at T_g + 50 °C because of its relatively high transmittance in the wavelength range from 250 to 350 nm. From the PL excitation and emission spectra, it was confirmed that these emissions at short wavelengths have small Stokes shifts, in contrast to the intrinsic luminescence of the non-heated $BaO–B_2O_3–SiO_2$ glass. From the PL decay curve of the 1% Pr-doped $BaO–B_2O_3–SiO_2$ glass obtained with heating at T_g + 50 °C, a fast decay component of 26.28 ns was estimated in the short wavelength range. These results indicate that the emissions in the short wavelength range were due to the 5d–4f transition of Pr^{3+} ions. The scintillation intensity of this fast emission was not high; however, the decay time is suitable for scintillator applications. The results of this study indicate that the crystallization of glasses can generate new luminescent centers that are suitable for scintillators.

Acknowledgments

This work was supported by Grants-in-Aid for Scientific Research A (17H01375), B (18H03468 and 19H03533), and Early-Career Scientists (20K20104) from Japan Society for the Promotion of Science. The Cooperative Research Project of the Research Center for Biomedical Engineering, Iketani Science and Technology Foundation, and Nippon Sheet Glass Foundation are also acknowledged.

References

1 G. F. Knoll: Radiation Detection and Measurement (Wiley, New York, 2010) 4th ed.
2 C. W. E. van Eijk: Nucl. Instrum. Methods Phys. Res., Sect. A **460** (2001) 1.
3 S. E. Derenzo, M. J. Weber, E. Bourret-Courchesne, and M. K. Klintenberg: Nucl. Instrum. Methods Phys. Res., Sect. A **505** (2003) 111.
4 C. W. E. van Eijk: Nucl. Instrum. Methods Phys. Res., Sect. A **529** (2004) 260.
5 C. W. E. van Eijk: IEEE T. Nucl. Sci. **59** (2012) 2242.
6 T. Yanagida: Opt. Mater. **35** (2013) 1987.
7 R. S. Holt, M. J. Cooper, and D. F. Jackson: Nucl. Instrum. Methods **221** (1984) 98.
8 K. Watanabe, K. Matsumoto, A. Uritani, K. Hitomi, M. Nogami, and W. Kockelmann: Sens. Mater. **32** (2020) 1435.
9 C. W. E. van Eijk: Phys. Med. Biol. **47** (2002) R85.
10 C. L. Melcher: Nucl. Instrum. Methods Phys. Res., Sect. B, **40**/**41** (1989) 1214.
11 N. Kawaguchi, G. Okada, K. Fukuda, and T. Yanagida: Nucl. Instrum. Methods Phys. Res., Sect. A **954** (2018) 161518.
12 T. Yanagida, G. Okada, and N. Kawaguchi: J. Lumin. **207** (2019) 14.
13 S. W. S. McKeever: Thermoluminescence of Solids (Cambridge University Press, Cambridge, 1985).
14 E. G. Yukihara and S. W. S. McKeever: Optically Stimulated Luminescence (Wiley, Chichester, UK, 2011).
15 S. W. S. McKeever: Nucl. Instrum. Methods Phys. Res., Sect. B **184** (2001) 29.
16 Y. Miyamoto, T. Yamamoto, K. Kinoshita, S. Koyama, Y. Takei, H. Nanto, Y. Shimotsuma, M. Sakakura, K. Miura, and K. Hirao: Radiat. Meas. **45** (2010) 546.
17 H. Nanto, Y. Miyamoto, T. Oono, Y. Takei, T. Kurobori, and T. Yamamoto: Procedia Eng. **25** (2011) 231.
18 Y. Miyamoto, H. Nanto, T. Kurobori, Y. Fujimoto, T. Yanagida, J. Ueda, S. Tanabe, and T. Yamamoto: Radiat. Meas. **71** (2014) 529.
19 N. Kawaguchi, H. Kimura, M. Akatsuka, G. Okada, N. Kawano, K. Fukuda, and T. Yanagida: Sens. Mater. **30** (2018) 1585.
20 T. Yanagida, H. Masai, M. Koshimizu, and N. Kawaguchi: Sens. Mater. **31** (2019) 1225.
21 Y. Fujimoto, K. Saeki, D. Nakauchi, T. Yanagida, M. Koshimizu, and K. Asai: Sens. Mater. **31** (2019) 1241.
22 D. Nakauchi, N. Kawaguchi, and T. Yanagida: Sens. Mater. **31** (2019) 1249.
23 H. Fukushima, D. Nakauchi, N. Kawaguchi, and T. Yanagida: Sens. Mater. **31** (2019) 1273.
24 M. Akatsuka, D. Nakauchi, N. Kawaguchi, and T. Yanagida: Sens. Mater. **31** (2019) 1289.
25 N. Kawaguchi, N. Kawano, G. Okada, and T. Yanagida: J. Lumin. **206** (2019) 634.
26 T. Yanagida, Y. Fujimoto, M. Arai, M. Koshimizu, T. Kato, D. Nakauchi, and N. Kawaguchi: Sens. Mater. **32** (2020) 1351.
27 P. Kantuptim, M. Akatsuka, M. Koshimizu, D. Nakauchi, T. Kato, N. Kawaguchi, and T. Yanagida: Sens. Mater. **32** (2020) 1357.
28 M. Akatsuka, D. Nakauchi, T. Kato, N. Kawaguchi, and T. Yanagida: Sens. Mater. **32** (2020) 1373.
29 D. Nakauchi, T. Kato, N. Kawaguchi, and T. Yanagida: Sens. Mater. **32** (2020) 1389.
30 Y. Takebuchi, H. Fukushima, D. Nakauchi, T. Kato, N. Kawaguchi, and T. Yanagida: Sens. Mater. **32** (2020) 1405.
31 N. Kawaguchi, G. Okada, Y. Futami, D. Nakauchi, T. Kato, and T. Yanagida: Sens. Mater. **32** (2020) 1419.
32 H. Kimura, T. Kato, D. Nakauchi, M. Koshimizu, N. Kawaguchi, and T. Yanagida, Sens. Mater. **31** (2019) 1265.
33 H. Kimura, D. Nakauchi, T. Kato, N. Kawaguchi, and T. Yanagida: Sens. Mater. **32** (2020) 1381.
34 T. Kato, D. Nakauchi, N. Kawaguchi, and T. Yanagida: Sens. Mater. **32** (2020) 1411.
35 D. Maruyama, S. Yanagisawa, Y. Koba, T. Andou, and K. Shinsho: Sens. Mater. **32** (2020) 1461.
36 S. Yanagisawa, D. Maruyama, R. Oh, Y. Koba, T. Andoh, and K. Shinsh: Sens. Mater. **32** (2020) 1479.
37 A. Ishikawa, A. Yamazaki, K. Watanabe, S. Yoshihashi, A. Uritani, Y. Sakurai, H. Tanaka, R. Ogawara, M. Suda, and T. Hamano: Sens. Mater. **32** (2020) 1489.
38 N. Kawaguchi, D. Nakauchi, S. Hirano, N. Kawano, G. Okada, K. Fukuda, and T. Yanagida: Jpn. J. Appl. Phys. **57** (2018) 02CB13.
39 N. Kawaguchi and T. Yanagida, Sens. Mater. **31** (2019) 1257.
40 D. Shiratori, Y. Isokawa, N. Kawaguchi, and T. Yanagida: Sens. Mater. **31** (2019) 1281.
41 H. Masai, H. Ofuchi, G. Okada, N. Kawaguchi, and T. Yanagida: Sens. Mater. **31** (2019) 1297.
42 N. Kawaguchi and T. Yanagida: Jpn. J. Appl. Phys. **59** (2020) SCCB21.
43 D. Shiratori, D. Nakauchi, T. Kato, N. Kawaguchi, and T. Yanagida: Sens. Mater. **32** (2020) 1365.
44 N. Kawaguchi, K. Fukuda, T. Yanagida, Y. Fujimoto, Y. Yokota, T. Suyama, K. Watanabe, A. Yamazaki, and A. Yoshikawa: Nucl. Instrum. Methods Phys. Res., Sect. A **652** (2011) 209.

45 N. Kawaguchi, H. Kimura, Y. Takebuchi, D. Nakauchi, T. Kato, and T. Yanagida: Radiat. Meas. **132** (2020) 106254.
46 M. Koshimizu, T. Yanagida, R. Kamishima, Y. Fujimoto, and K. Asai: Sens. Mater. **31** (2019) 1233.
47 A. Horimoto, N. Kawano, D. Nakauchi, H. Kimura, M. Akatsuka, and T. Yanagida: Sens. Mater. **32** (2020) 1395.
48 S. Polosan, A.C. Galc, and M. Secu: Solid State Sci. **13** (2011) 49.
49 J. Jiang, G. Zhang, and M. Poulain: J. Alloys Compd. **275–277** (1998) 733.
50 J. Fu, J. M. Parker, P. S. Flower, and R. M. Brown: Mater. Res. Bull. **37** (2002) 1843.
51 M. Secu, C. E. Secu, S. Polosan, G. Aldica, and C. Ghica: J. Non-Cryst. Solids **355** (2009) 1869.
52 Z. T. Kang, R. Rosson, B. Barta, C. Han, J. H. Nadler, M. Dorn, B. Wagner, and B. Kahn: Radiat. Meas. **48** (2013) 7.
53 N. Kawaguchi, H. Masai, H. Kimura, G. Okada, and T. Yanagida: J. Non-Cryst. Solids **501** (2018) 126.
54 T. Yanagida, K. Kamada, Y. Fujimoto, H. Yagi, and T. Yanagitani: Opt. Mater. **35** (2013) 2480.
55 G. H. Beall and D. A. Duke: J. Mater. Sci. **4** (1969) 340.
56 I. I. Kindrat, B. V. Padlyaka, and A. Drzewieckia: J. Lumin. **187** (2017) 546.
57 D. Nakauchi, G. Okada, M. Koshimizu, N. Kawaguchi, and T. Yanagida: Physica B Condens. Matter **530** (2018) 38.
58 A. Zych, M. Lange, C. M. Donegá, and A. Meijerink: J. Appl. Phys. **112** (2012) 013536.